ADVANCED ENGINEERING MATERIALS

DOI: 10.1002/adem.201700062

Is it Possible to Use Rolling Methods to Improve Textures on Fe–Mn–Si Shape Memory Alloys?**

By *Ana V. Druker, César Sobrero, Valeria Fuster, Jorge Malarría* and *Raúl Bolmaro**

No uniform rolling deformation produces shear strains that give rise to textural and microstructural heterogeneities in processed metals and alloys. In this work, the authors investigate Fe–30Mn–4Si shape memory alloy sheets rolled in different conditions at 600 °C, in order to determine the process giving rise to the best structure and the strongest {100}<110> shear texture. This crystallographic orientation is the most favorable for the $\gamma \rightarrow \varepsilon$ martensitic transformation, which provides the shape memory effect in these alloys. In the current conditions, the authors find that unidirectional rolling produces a shear texture in sheet's surface layers. The authors compare the texture and microstructure from this process to those obtained from reverse rolling and single-roller drive rolling.

1. Introduction

It is well known that the shape memory effect (SME) of ferrous alloys is due to a $\gamma_{(FCC)} \rightarrow \varepsilon_{(HCP)}$ martensitic transformation which takes place by the selective movement of a single variant of the a/6 [112] Shockley partial dislocations on {111} austenite planes. The activation of a single variant of partial dislocations is essential because the transformation would produce no significant macroscopic dimensional changes if all of the 12 equivalent types of partial dislocations were activated. To activate just one of the preferential variants, deformation must be driven by an external stress.[1,2] If the other conditions that influence the process are sufficiently controlled, a later heating above the A_f temperature will induce the $\varepsilon \rightarrow \gamma$ inverse transformation through the same crystallographic path with the forward transformation in the opposite direction.[3] Thus, the material will return to its initial dimensions.

To maximize the SME, it is important that the parent austenite phase does not deform plastically before the martensitic transformation starts due to the applied stress. In other words, the resolved shear stress (τ_R) on the {111}<110> slip system, must not reach the critical resolved shear stress (τ_{CR}) before the τ_R on the {111}<112> reaches the $\gamma \rightarrow \varepsilon$ transformation stress ($\tau_{\gamma \rightarrow \varepsilon}$). In this regard, Sato et al.[4] showed the following relationships between crystallographic orientation and SME in single crystals:

1) The SME is almost perfect if the tensile stress is applied in the <441> direction, producing the highest Schmid factor, 0.5, on only one variant of the {111}<112> system,
2) If the tensile stress is applied in the <100> direction, while holding all other conditions constant, the SME is strongly suppressed.

Based on these results, it is reasonable to expect that a favorable polycrystal texture will improve the SME in industrial alloys.

Matsumura et al. obtained a shear texture, <110>//RD fiber, in the external layers of their Fe–28Mn–6Si–5Cr–0.03C sheets by conducting the final rolling passes at a low temperature of 850 °C.[5,6]

Stanford et al. found that the SME, measured in bending in an Fe–13Mn–5Si–9Cr–7Ni–0.03C alloy, is affected by the orientation of the test strip in relation to the rolling direction.[7] They showed that the best performing testing orientation has the <110> direction aligned perpendicular to the bending tensile direction. Recently, Fu et al. investigated the evolution of cold-rolling and recrystallization textures in shape memory alloys and discussed the improved superelasticity phenomenon on this severe cold-rolled material.[8]

[*] *Prof. Dr. R. Bolmaro, Prof. Dr. A. V. Druker, Dr. C. Sobrero, Dr. V. Fuster, Prof. Dr. J. Malarría*
Facultad de Cs. Ex., Ingeniería y Agrimensura (UNR), Av Pellegrini 250, 2000 Rosario, Argentina
Instituto de Física Rosario (CONICET-UNR), Bv. 27 de Febrero 210 bis, 2000 Rosario, Argentina
E-mail: bolmaro@ifir-conicet.gov.ar

[**] *This research was funded by the Consejo Nacional de Investigaciones Científicas y Técnicas and Agencia Nacional de Promoción Científico-Tecnológica of Argentina. The authors would like to thank Mr. Fernando Ugo for his assistance with the mechanical tests and Dr Michel Stout for a critical reading of the manuscript.*

They found that 98.5% cold-rolled FeNiCoAlNbB alloy with strong {hk0}⟨001⟩ recrystallization texture, followed by aging for 96 h at 600 °C, exhibited a superelasticity of 3.2% with a residual strain of only 0.7%, and a tensile strength of approximately 960 MPa. Compared with the non-superelastic behavior of the as-forged FeNiCoAlNbB alloy, the considerably improved superelasticity is mainly attributed to the formation of strong favorable textures and the suppression of grain boundary precipitation.

Besides, other factors affect the SM behavior. The stacking fault energy (SFE) must be low enough, so dislocations may dissociate in partials, resulting on a fine distribution of stacking faults, nuclei of ε-martensite. On the other hand, some dislocations in the austenite grains should harden the matrix, avoiding plastic deformation when the stress to induce the martensitic transformation is applied.

In a previous work, we investigated the influence of rolling temperature on the SME in an Fe–30Mn–4Si alloy and found that the sheets rolled at 600 °C and annealed at 650 °C exhibited the best shape recovery with respect to the material rolled at room temperature and at 1000 °C.[9] We kept the rolling reductions, lubricant conditions between rolls and sheets, and geometries almost equal for all temperatures. The surface of samples rolled at both 600 and 1000 °C developed a shear texture in the austenitic FCC phase, with a strong {001}<110> component, near the best <441> direction (Figure 1). During tensile deformation, those favorable texture components disappeared from the remaining austenite while ε-martensite formed.

Lee and Duggan proposed that the texture differences would likely result from temperature influence on SFE.[10] The SFE of this alloy is low at 20 °C (22 mJ m^{-2}), which promotes twinning as a favorable deformation mode. By following those authors, twinning followed by shear banding and slip, would give rise to high deformation rolling textures of the kind {110}<112> and {110}<001> plus a minor {111}<*uvw*> component. If the shear component {001}<011> were formed by slip, it would twin to a {122}<411> orientation. Then the twin-matrix structure would rotate to {100}<001> or {111}<*uvw*> (Figure 1a). These texture components are not

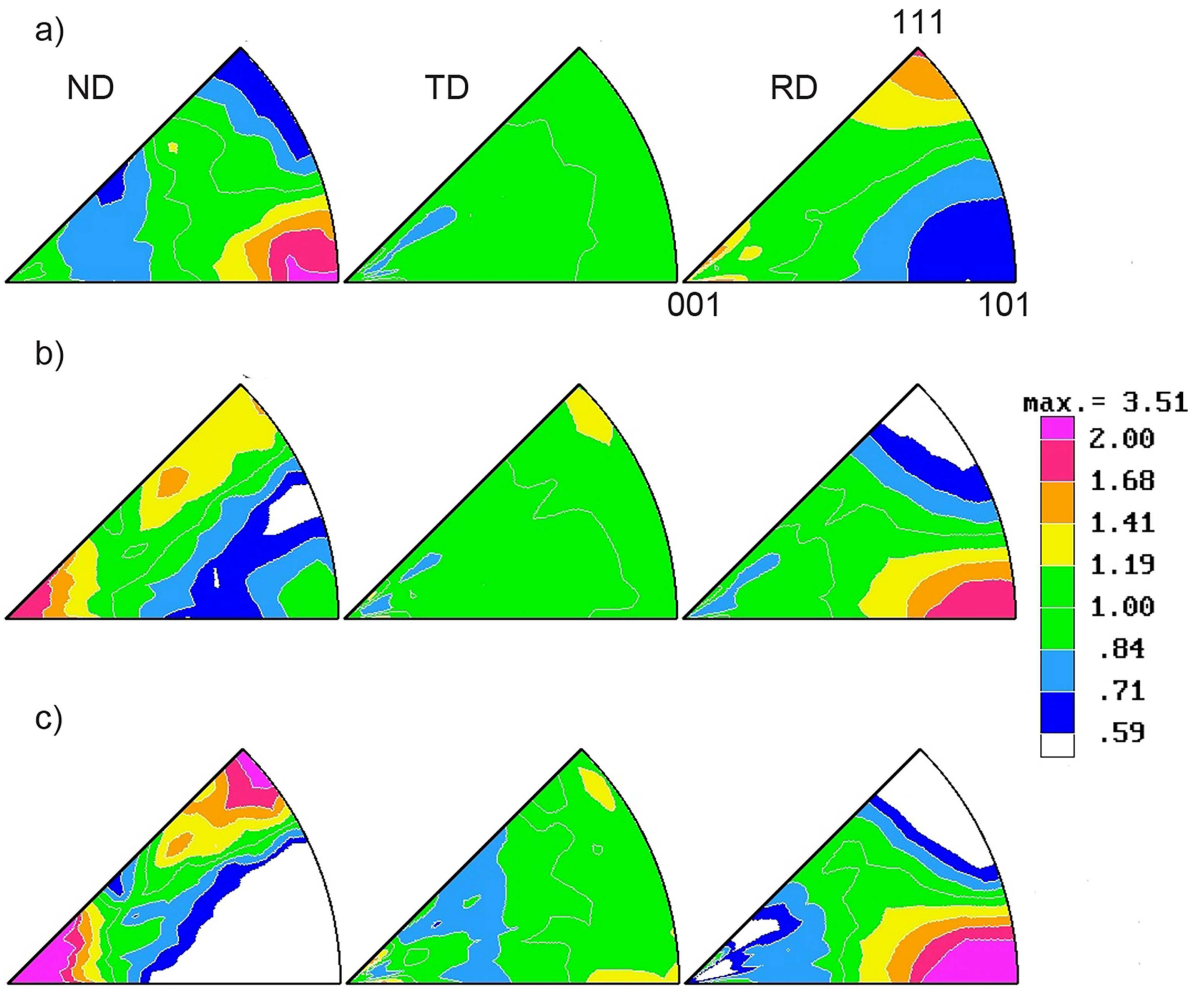

Fig. 1. Inverse pole figures measured on the surface of an Fe–30Mn–4Si alloy unidirectional rolled at: (a) room temperature, (b) 600 °C, (c) 1000 °C.[8]

ADVANCED ENGINEERING MATERIALS 2017,
DOI: 10.1002/adem.201700062

ADVANCED ENGINEERING MATERIALS

observed in the surface of the sheets rolled at 600 and 1000 °C (Figure 1b, c) probably because the alloy has a higher SFE at these temperatures and thus the shear component {001}<011> remains. In addition, increasing frictional stresses between the sheet and rolls with temperature could increase shearing and contribute to inhomogeneous deformation.

Looking for shear texture, many authors studied the effect of various rolling techniques as symmetric, asymmetric, continuous, snake, and reversed rolling in different materials.[11–19] Equal Channel Angular Extrusion (ECAE), is also a fundamentally shearing deformation process, used for developing characteristic textures on many metals and alloys.[20–28]

Current authors have used ECAE to develop textures favorable to improve the degree of shape recovery (DSR), since the material has a large <110> component, near the ideal <441>, in the extrusion direction.[29] However, ECAE is not an industrial continuous deformation process generally accepted for fabrication purposes.

This work is devoted to investigate some variations on the rolling process at 600 °C, to determine the conditions providing both the strongest shear texture components and a shear effect acting deeper on Fe–30Mn–4Si samples, which might favor the $\gamma \rightarrow \varepsilon$ transformation, and also the best microstructure.

2. Experimental Section

We prepared an Fe–30Mn–4Si (wt%) alloy in an induction furnace under protective argon atmosphere, homogenizing it at 1000 °C for 3 h with further slow cooling. Subsequent to fabrication, we deformed the ingots to a thickness of 1 mm, according to the following rolling schedules:

Sample UR: successive unidirectional rolling passes at 1000 °C reducing the thickness from 10 to 1.6 mm followed by 37% total reduction into 1 mm at 600 °C in multiple steps.

Sample SR: single-roller drive rolling passes at 1000 °C reducing the thickness from 10 to 1.6 mm (0.2 mm reduction per pass) followed by 37% total reduction into 1 mm at 600 °C (0.1 mm reduction per pass).

Sample RR: successive reverse rolling passes at 1000 °C reducing the thickness from 10 to 1.6 mm followed by 37% reduction at 600 °C in multiple steps.

The rolling speed and roll diameters were 16.65 rpm and 86 mm, respectively. To measure the velocity of the idle roll in single-roller drive rolling (**SR**), we prepared a video recording the complete passage of the sheet through the rolling mill, and analyzed the frames one by one to identify the moment when the idle roller starts to move. Each frame of the video was saved as an individual file. Then, we input the images into Adobe Photoshop and superimposed these files forming one graphic, which showed the positions of the white mark on both rollers at two different moments in time. The angle between the marks indicates the distance traveled during the time interval between images. In this way, we calculated the "almost instantaneous" rolling speed.

We found that in 0.23 s, the idle roller is accelerated due to friction with the sheet being rolled up to a speed equal to that of the driven roller. In Figure 2, we show intervals of approximately 52° of driven roller movement, corresponding to the stepping stages, in single-roller drive rolling at 1000 and 600 °C. The results confirm that both rolls spin at the same speed, when rolling at high temperature. On the other hand at 600 °C, the driven roller moves at 0.079 m s^{-1}, while the idle roller goes more slowly, at 0.070 m s^{-1} through an angle of 47°.

The friction governs these behaviors, which depends on lubrication, work material, and working temperature. In cold rolling, the friction coefficient value is around 0.1, the condition is called *sliding friction*. In warm working, a typical value is around 0.2; and in hot rolling, it is around 0.4.[30] Hot rolling is characterized by a condition called *sticking*, in which the hot work surface adheres to the rolls over the contact arc. When sticking occurs, the coefficient of friction can reach 0.7, and, as a consequence, the surface layers of the sheet are restricted to move at the same speed as the driven roll speed; and below the surface, deformation is more severe allowing passage of the piece through the roll gap.

After rolling, samples were water quenched and subsequently annealed at 650 °C for 20 min.

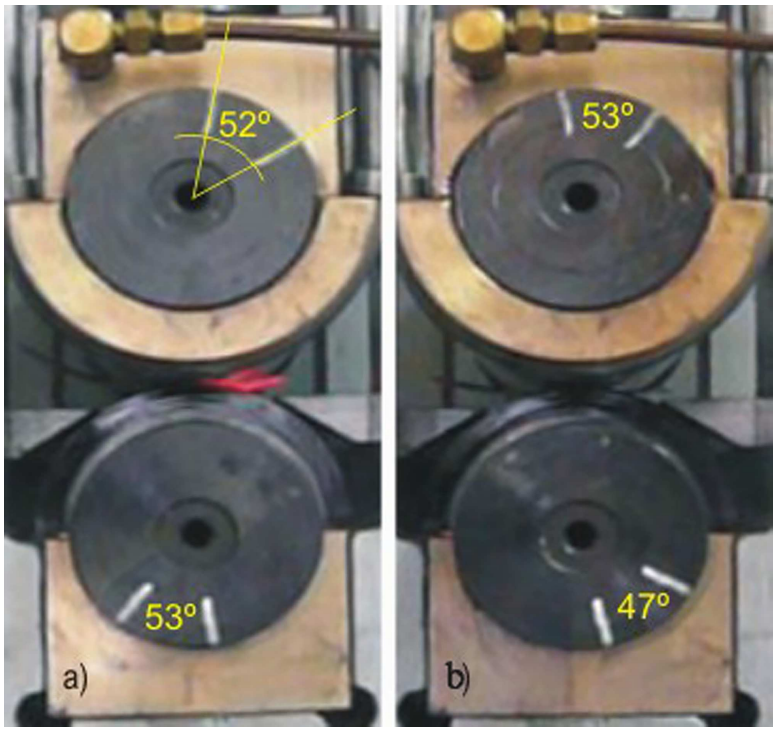

Fig. 2. Measurement of rolls' rotation in single-roller drive rolling regimen, at different temperatures: (a) 1000 °C, (b) 600 °C.

DOI: 10.1002/adem.201700062

Microstructural analysis were performed using a PME3 Olympus optical microscope equipped with a NIC device, and a Philips CM200 transmission electron microscope (TEM) operating at 200 kV with an ultra-twin objective lens. Specimens for transmission electron microscopy (TEM) were mechanically thinned to 0.2 mm, then electropolished by using the double jet technique with a 90/10% acetic/perchloric electrolyte at room temperature.

Surface texture measurements were made on $20 \times 12 \times 1$ mm thickness samples. The specimens were mechanically polished to 600 grit and then electropolished with an 80/20% acetic/perchloric solution. The through thickness variation of the texture was also measured by careful reduction of the thickness with emery paper and further electropolishing to eliminate the layer affected by the mechanical grinding. That procedure was always necessary because this alloy is susceptible to stress induced martensitic transformation during rough dressing.[31] X-ray pole figures were determined using Cu-$K\alpha_1/K\alpha_2$ lines in a Philips X-pert pro MPD goniometer. The low penetration capabilities of copper radiation in ferrous alloys (approx. 10 μm) is usually considered a disadvantage that was turned on an advantage in our case allowing the measurement of texture variations with very small depth sampling. The initial data was corrected for defocusing and further analyzed by WXpopLA (the current Windows 7 implementation of the popLA software).[32]

To determine the shape memory properties, we tensile deformed the different samples in an Instron 3362 universal testing machine. The specimens were machined out of the 1 mm thickness sheets parallel to the rolling direction by means of wire electrical discharge machining. The specimen's geometry was defined according to ASTM E8 standard with a gauge length of 25 mm and the results represent the average SME through the whole thickness. The quantity of martensite was determined by the Rietveld method, which incorporates the full texture, or preferred orientation, analysis into the traditional refinement. The MAUD program (Material Analysis Using Diffraction http://maud.radiographema.com/) was used. The reverse transformation was obtained by heating at 500 °C for 20 min, i.e., above A_f temperature, under an argon atmosphere. The sample lengths were measured between two indentation marks made with a Shimadzu micro hardness device. The *DSR* was calculated as:

$$DSR = \frac{l_2 - l_1}{l_1 - l_0} \cdot 100 \quad (1)$$

where, l_0, l_1, and l_2 are the initial probe length, the length after deformation, and the length after reverse transformation, respectively.

3. Results and Discussion

3.1. Texture Evolution

Figure 3 shows the {111} pole figures measured on TD-RD planes at different depths from the surfaces, and later on tilted to show results as if they were seen on ND-RD planes. The great advantage of this view is that shearing deformation becomes clearer than from the top of the sheet, but we still keep the scanned volume limited to a thin layer of inspection. Besides, any X-ray technique scanning on the lateral side of the sheets (ND-RD) would average the textures through the whole thicknesses. Figure 3a corresponds to sample **UR -**the sheet unidirectional rolled at 600 °C and then annealed at 650 °C- at a depth of 0.13 mm; in this position we found a typical FCC shear texture, as was anticipated in Figure 1b. At a depth of 0.22 mm that texture degrades, leading to a typical *brass* FCC rolling texture at a depth of 0.25 mm, which is stronger at the sheet center.

Inverse pole figures corresponding to each depth (Figure 4) give the following information:

1) At a depth of 0.13 mm, the principal texture components are {001}<110> and {111}<110>.
2) Away from the sheared surface regions, the texture evolves into a random distribution of crystallographic orientations.
3) Between a depth of 0.25 mm and the sheet's center, a typical rolling texture (β fiber), consisting in {101}<111> is present.

Formation of the localized textures can be attributed to two effects that produce shear deformation, roll gap geometry and friction between the rolls and the sheet, which implies a velocity gradient along the sheet thickness. Figure 5 is a schematic diagram of both effects showing the evolution of a differential element during rolling deformation. As it can be seen in the figure, the shear stresses present maxima at the roll sheet interface, so being both effects present, the surface texture will be different from that in the sheet interior whenever the shearing strains are not closely compensated, leaving a prevalence of the shearing component over the pure elongation. According to Lee and Duggan, an inhomogeneous texture suggests that the strain ratio $\frac{e_{13}}{e_{11}} \geq 0.5$ in this sample.[10]

The combination of all texture components present through the thickness is shown in Figure 6a and 7a, by pole figure and inverse pole figure averages, respectively. It can be seen that the {uvw}<110> components are relatively weak.

Figure 3b shows pole figures from sample **SR**, measured across the specimen thickness from the surface in contact with the driven roll to the opposite surface, in contact with the idle roll. Each section in Figure 3b has a typical rolling texture, with components stronger than in the previous sample, **UR**. There is no evidence of the existence of {uvw}<110> components either on the averaged pole figures or inverse pole figures (Figure 6b, 7b). It is well known that the rotating speed of the idle roll cannot be prescribed, but may be determined by the fact that the rolling torque is zero. It is usually argued that the idle roll rotates at a speed slower than the driven roll, mainly influenced by friction forces on the rolling gadget itself counteracting the transmission by friction from the driven roll through the metal sheet. Therefore, the shear deformation is induced because of the speed distribution, and some shear texture should be observed at the center

DOI: 10.1002/adem.201700062

ADVANCED ENGINEERING MATERIALS

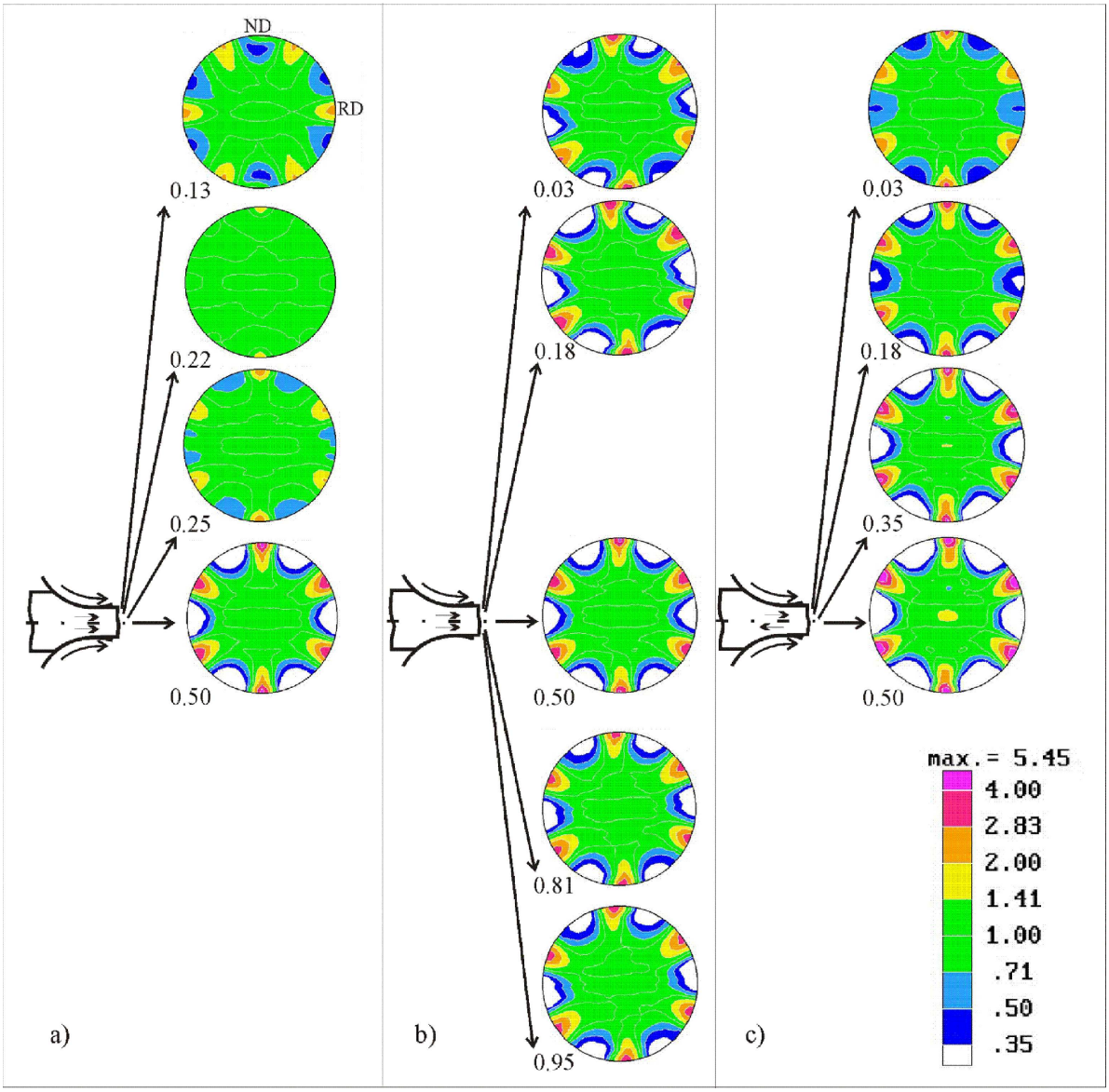

*Fig. 3. {110} pole figures taken at descending depths from the sample surface of: (a) sample **UR**, (b) sample **SR**, (c) sample **RR**. Arrows on the rolls indicate their direction of rotation. Little arrows on the sheets indicate pass directions.*

of the thickness. Why normal rolling texture is observed in our experiment? Most authors apply **SR** to soft materials, rolled at room temperature with high reductions.[12,13,17] In contrast, our hard alloy ($HRc \cong 30$) is rolled at 600 °C to obtain the necessary reduction and appropriate microstructure in many passes. In these conditions, we supposed that, while the sheet is rolled it transmits the effort from the driven roll to the idle one, inducing it to rotate at the same velocity. Thus, all planes between the two roll surfaces would have the same velocity. Without through thickness velocity gradient, there are no shear strain components in the material. To measure the velocity, we recorded videos and evaluated the rotation angle while sheets were rolled. At 600 °C in 0.23 s, the idle roll almost matches the driven roll velocity. Table 1 shows the velocity of the idle roll when rolling was performed at different temperatures and at the same velocity of the driven roll.

Experiments have showed that both rolls moved at the same velocity when rolling was performed at high and medium temperatures, at which the material suffers a greater oxidation. On the other hand, at low temperatures, friction coefficient reduces and probably the "sliding friction" phenomenon occurs. The composition of the oxide scale depends on the temperature at which it forms; so the scale layer can act as a lubricant or as a friction-enhancing medium.[33]

According to Mac Gregor and Coffin's results, we assumed it would be possible to find a shear texture in the sheet center, if we alternate the rolling sense between passes.[34] We explored that route and Figure 3c shows pole figures of sample **RR**, measured at different depths from the specimen's

DOI: 10.1002/adem.201700062

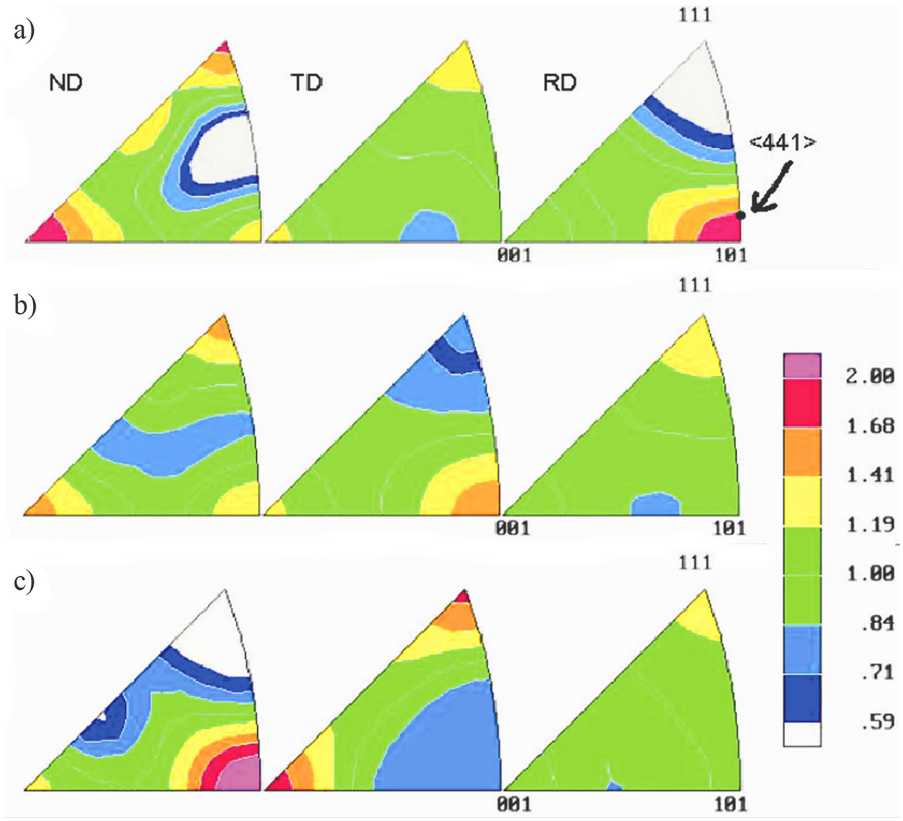

Fig. 4. Inverse pole figures of sample ***UR*** *at descending depths from surface: (a) 0.13 mm, (b) 0.22 mm, (c) 0.25 mm.*

surface to the center. Figure 6c and 7c show pole figures and inverse pole figures, respectively, averaged over the sheet thickness. There are none {uvw}<110> texture components in the sheet rolled under these conditions, showing that shear deformation is actually a minimum all through the sample thickness.

3.2. Shape Memory Effect

Figure 8 shows stress-strain curves for samples **UR**, **SR**, and **RR**, 3.5% deformed in tension. As can be seen in Table 2, the values of the stress that induces $\gamma \rightarrow \varepsilon$ martensitic transformation, $\sigma_{\gamma \rightarrow \varepsilon}$, do not vary substantially despite the different way of processing and resultant texture. The important factor is not the apparent yield stress, but how yielding happens: by production of ε-martensite or irreversible plastic flow. Figure 9 shows the XRD patterns obtained from the tensile samples. Austenite and ε-martensite phases are identified by its traditional Greek symbol, followed by the Miller indices *(hkl)* of the corresponding set of planes satisfying the diffraction condition. The fractions of ε-martensite determined by refinement of the diffractograms are also summarized in Table 2.

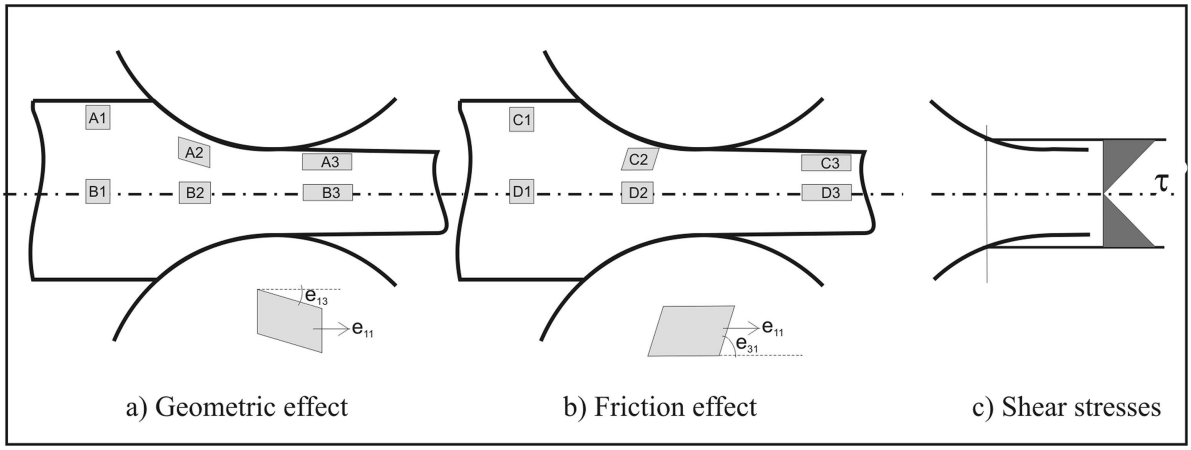

Fig. 5. (a) and (b): Deformations on the differential elements A1, B1, C1, and D1 during the rolling process, (c) the resulting shear stresses distribution.

DOI: 10.1002/adem.201700062

ADVANCED ENGINEERING MATERIALS

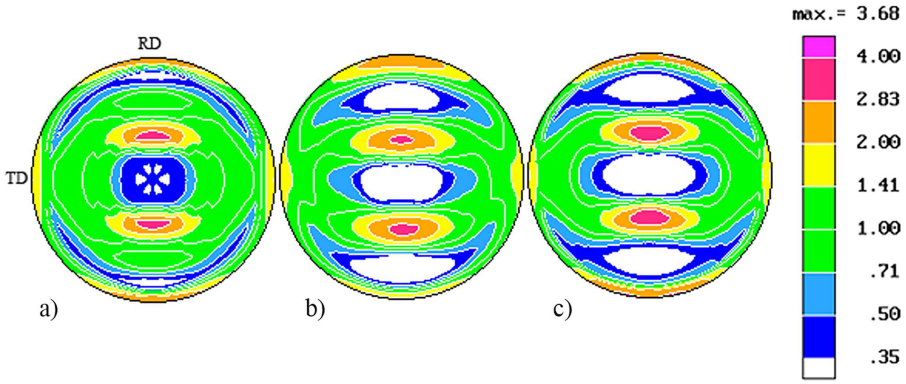

*Fig. 6. {111} pole figure averages of: (a) sample **UR**, (b) sample **SR**, (c) Sample **RR**.*

In order to evaluate the SME, the tensile specimens were heated at 500 °C for 20 min. Comparison between the different cases indicates that the DSR is higher for the sample with shear texture components (**UR**), although the amount of ε-martensite is much lower than those induced in sheets rolled by non-conventional methods. In this case, the applied stress may have induced mainly the $\gamma \rightarrow \varepsilon$ transformation; on the other hand, samples with low DSR could suffer plastic deformation on the austenitic phase or, alternatively, the inverse transformation proceeded through $\varepsilon \rightarrow \gamma$ variants different from the one active on forward transformation.

The low volume fraction of ε-martensite could be due to the introduction of plates on only one favorably oriented {111} plane variant per grain, which activates while the specimen elongates. When martensite plates are introduced on more than two variants, they self-accommodate through a lot of redundant deformation, and the macroscopic deformation is

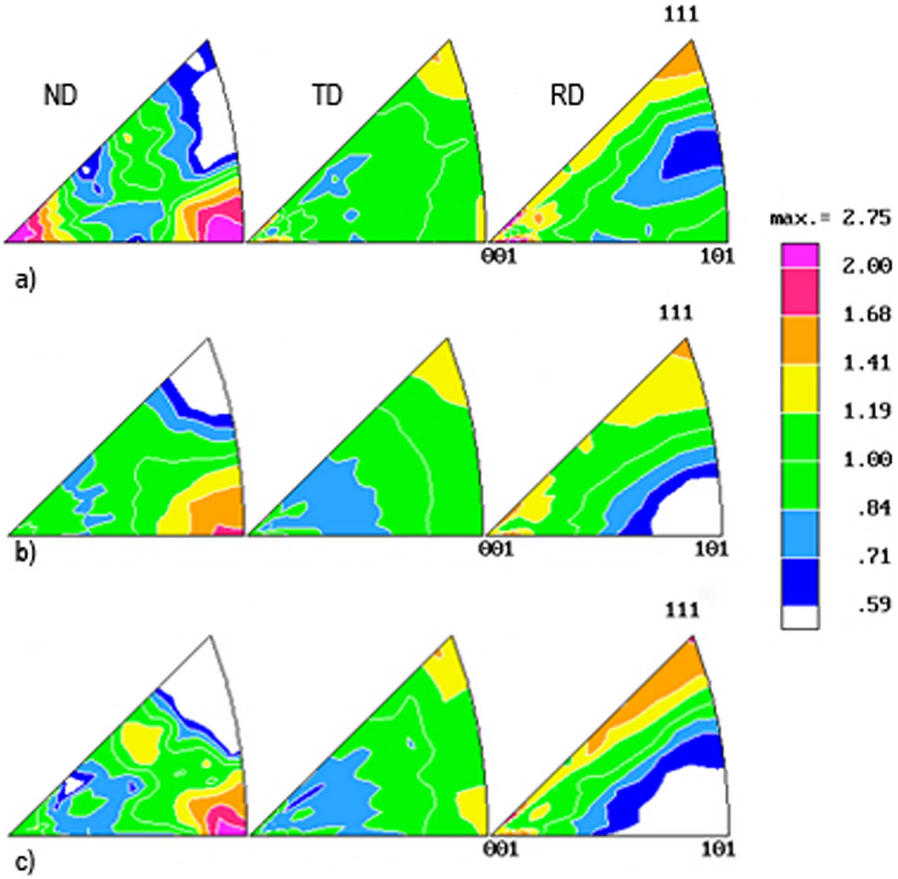

*Fig. 7. Inverse pole figure averages taken from three orthogonal orientations of: (a) sample **UR**, (b) sample **SR**, (c) Sample **RR**.*

DOI: 10.1002/adem.201700062

*Table 1. Idle roll velocity in single-roller drive rolling (**SR**), with a driven roll velocity of 0.079 m sec^{-1}.*

Rolling temperature [°C]	Velocity [m sec^{-1}]
1000	0.079
600	0.078
400	0.067

Table 2. Stress that induces permanent deformation ($\sigma_{0.2}$), percent of tensile deformation ($\in$), percent of ε-martensite induced after the tension tests and Degree of Shape Recovery (DSR).

Sample	$\sigma_{0.2}$ [MPa]	$\in$ [%]	ε-martensite [%]	DSR [%]
UR	490–555	3.3	20	55–57
SR	448–450	3.4	57	24–25
RR	400–440	3.6	73	19–28

achieved through two mechanisms: additional martensitic transformation and perfect dislocation slip in both phases. Sato et al. suggested that the reverse transformation by the motion of partial dislocations, thorough the same path of direct transformation, is hindered by the ε-plates formed on the different {111} planes.[4] Metallographic evidence for this will be presented later.

How texture affects both mechanisms? A texture component {001}<110> means that the <110> directions are nearly aligned with the rolling (RD) and transverse directions (TD) and, additionally, the <100> direction will lie at 45° to the RD, in the majority of the grains. As speculated by Matsumura et al., if a tensile stress is applied along the RD, those austenitic grains oriented near [110]//RD may transform to ε−martensite on the variant of the (111)[$\bar{2}$11] system with the highest Schmid factor.[5] They argue further that, when this transformation is produced, the tensile axis rotates from the [110] direction to the [$\bar{2}$11] direction (near to [441]), increasing the Schmid factor of the slip system. As the Schmid factor increases, the martensitic transformation on the single variant (111)[$\bar{2}$11] accelerates, which is essential for achieving a good SME. Contrarily, when grains with a <001> direction parallel to tensile axis, begin to transform on a single ($\bar{1}$11)[$\bar{1}$12] variant system, the specimen axis rotates from [$\bar{1}$18] to [$\bar{1}$12], thus decreasing the Schmid factor. Consequently, the other three variants also operate and the axis maintains its original macroscopic orientation. This argument follows Sato's explanation of SME degradation when ε−martensite is formed in more than two {111} planes.[4] Therefore, the rolling condition that orients the sample axis, such that the tensile stress is parallel to the directions <110>, <441>, and <221>, produces the most favorable conditions for a good SME. We previously showed that a nearly ideal <441> direction lying parallel to RD disappears, when samples are deformed in tension.[9] The disappearance of the <441> component indicates that the martensitic transformation proceeds easier for that orientation.

Among the studied cases in the current work, this condition only was found in the unidirectional rolled sample

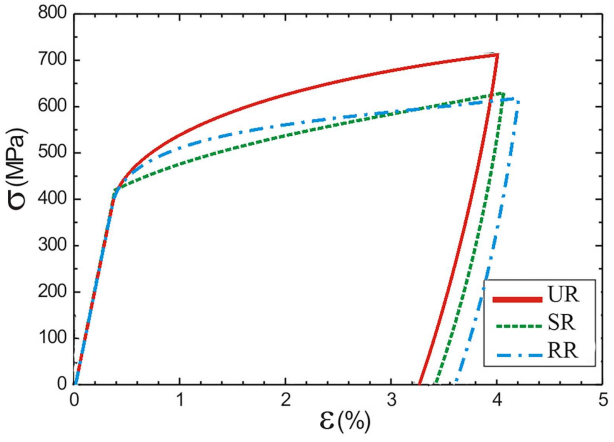

*Fig. 8. Stress–strain curves for samples **UR**, **SR**, and **RR**.*

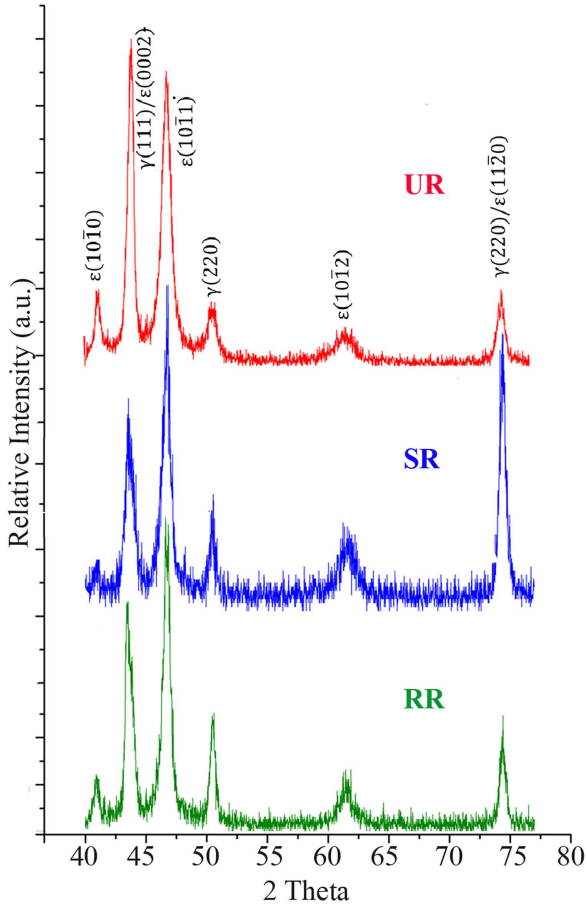

Fig. 9. X-ray patterns obtained from the tensile samples. The planes and phases are identified by Greek symbols followed by the Miller indices (hkl).

ADVANCED ENGINEERING MATERIALS **2017**,
DOI: 10.1002/adem.201700062

ADVANCED ENGINEERING MATERIALS

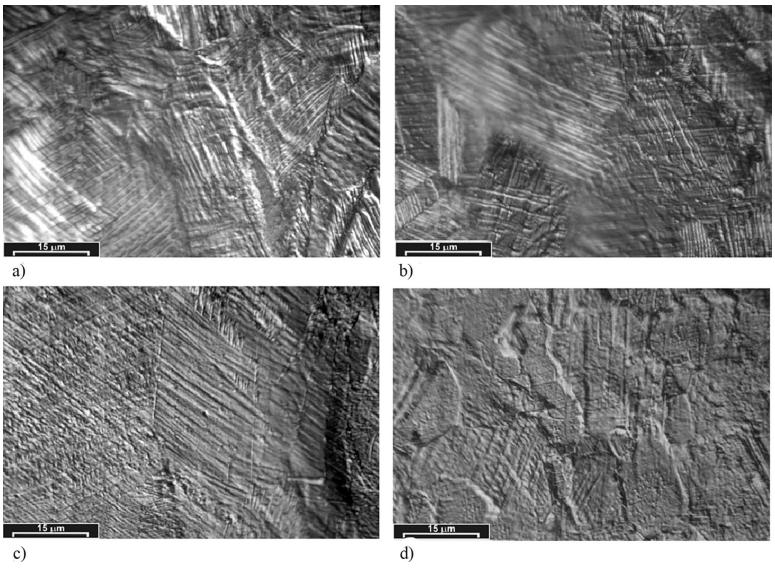

*Fig. 10. OM images of: (a) the unidirectional rolled material (**UR**), (b) the single-roller driven rolled material (**SR**), and (c) the reversely rolled material (**RR**), all showing martensite plates in the austenite matrix after 3% tensile deformation; and (d) the **SR** material showing the austenite matrix after reverse transformation.*

(**UR**), in contraposition with our expectations about modifying textures in the right way by applying asymmetric or reverse rolling (**SR** or **RR**).

3.3. Microstructural Analysis

The material's microstructure was analyzed by optical metallography after 3% deformation in uniaxial tension. The ε-martensite plates on one type of {111} plane are clearly observed in Figure 10a taken from the **UR** sample. This is especially true for the grains, where the transformation was presumably favored by the relationship between the grain orientation and the tensile axis. A feature of stress-induced martensite is the curved shape of the plates. Such an aspect distinguishes this martensitic form from thermal martensite, where the plates stop at the grain boundaries and the austenite-martensite interface is more strongly defined.[18] The refined plate morphology corresponds to a matrix with a high defect density, as it will be seen in TEM images. Some defects act as nucleation sites and others hamper the growth of the martensite.

Figure 10b, taken after 3% tensile deformation, shows that more than two variants of martensite plates developed in the different grains of the **SR** sample.

The sheet processed by reverse rolling (**RR**) had a microstructure consisting of elongated grains and small twins. After 3%, tensile deformation the specimens contained a large quantity of martensite plates on more than two variants (Figure 10c).

After the reverse-transformation, only γ phase X-ray reflections were observed in the diffractograms. Reliefs remaining on the positions of the already retransformed original martensite plates are observed in the **SR** and **RR** sample (Figure 10d). Many active martensite variants produce the retransformation by a path different from the direct one, resulting in a low degree of shape recovery.

Figure 11a–c show TEM microstructure of samples processed by **UR**, **SR**, and **RR**, respectively. All of them are annealed at 650 °C for 30 min. The first one shows dislocation bands in the γ phase, and fairly dense dislocation arrays among the bands. The **SR** sample shows a structure of dislocation cells; a sample taken from the surface (Figure 12) shows a detail of dislocations on the $(11\bar{1})[\bar{1}10]$ and $(1\bar{1}1)[\bar{1}01]$ systems and few stacking faults aligned along the traces of $(1\bar{1}1)$ planes and near $[21\bar{1}]$ or $[\bar{1}12]$ directions. Besides, the **RR** (Figure 11b) shows dislocation tangles that are not random but tent to form a Taylor lattice.

We have previously processed a ferrous SMA by ECAE and found a microstructure similar to that shown in Figure 11a, that is, stacking faults, accompanied by a high density of dislocations and deformation bands in the austenitic matrix.[29] As occurred in the **UR** sample, we expected a higher DSR. The texture developed by the severe deformation remained after annealing at different temperatures, while the recrystallized grains and a new defect distribution resulted in better shape recovery. The resultant texture was clearly beneficial for the shape memory properties, for what the current attempt was designed in search of a better-suited industrial procedure as rolling.

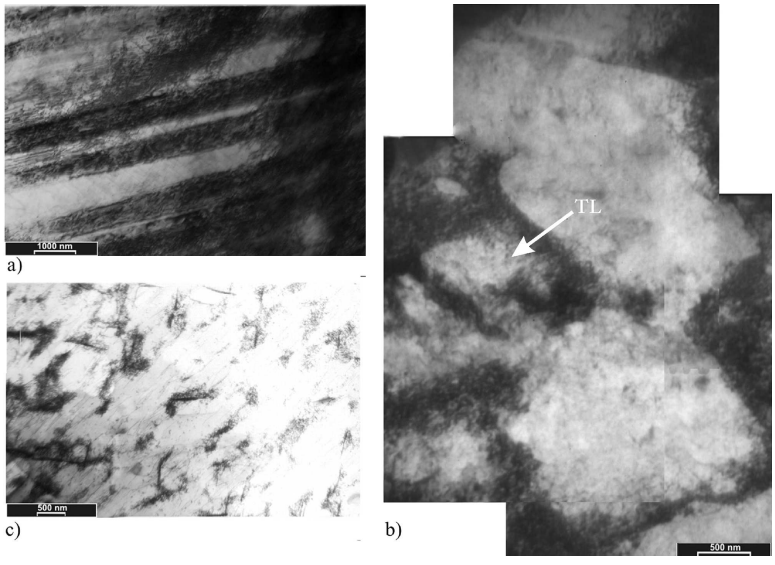

Fig. 11. TEM microstructure of sheets rolled at 600 °C: (a) unidirectional, (b) single-roller drive, (c) reverse; all of them are annealed at 650 °C. Taylor lattices in the RR sample are indicated by an arrow.

DOI: 10.1002/adem.201700062

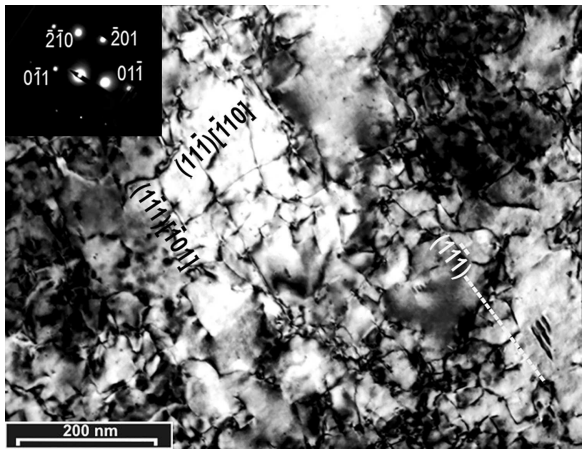

Fig. 12. Detail of the microstructure of the single-roller drive rolled sheet, annealed at 650 °C.

4. Conclusions

In this work, we performed different rolling schedules on Fe–Mn–Si alloy, analyzing the microstructure and the degree of shear texture, which is known to be favorable for the SME.

1) When unidirectional rolling is performed, inhomogeneous deformation at different depths from the surface leads to a {uvw}<110> texture component aligned with the RD. The stress induced ε-martensite plates on only one variant and the degree of shape recovery are the best among the studied cases.
2) When one of the rolls was idle, the sheet transmitted the movement from the driven roll and the same deformation velocity was established through the sheet thickness. Shear stresses at the lead in, when the sheet enter the rolls, disappear almost instantaneously, resulting in a typical rolling texture through the bulk of the material, even including the near surface region. The stress induced ε-martensite developed in more than two variants and the shape recovery is ∼25%.
3) If reverse rolling is performed while maintaining the rolling channel characteristics and percentage reduction, inhomogeneities are self-compensated and a typical rolling texture, without shear components, is present across the sheet thickness. The reverse transformation of the many variants of the martensite plates is almost hindered, and the degree of shape recovery reaches values between only 19–28%.
4) Optical micrographs showed a close correlation of the microstructure, volume fraction, and number of variants with values obtained by XRD and Rietveld analysis.
5) TEM observations of the dislocation structures show different kinds of arrays as a result of the deformation processes. When cells or tangles are present, they affect the movement of the partial dislocations. Those are the cases of single-roller drive and reverse rolled specimens, in which the degree of shape recovery is quite poor.
6) So far, the easier shape recovery cannot be unmistakable taken as a consequence of only the shearing texture, a rather macro effect, or only the absence of cells or tangles, microstructural features that are apparently due to pure shear deformation.

Unfortunately, the texture apparently favoring the $\gamma \rightarrow \varepsilon$ transformation exhibits a marked gradient through the sheet's thickness. The preferred texture is largely absent at the sheet's center, although relatively strong near the surface and probably with the intermediate orientations also favoring the presence of SME. A great effort should be devoted to increase the volume fraction of shear components toward the inner layers of the sample, as a way of fixing at least that variable and investigate the possible relationship between absence of shearing deformation and microstructural features precluding shape recovery.

Additionally, we can conclude that hard materials as the current one are not prone to develop shearing textures when solicited by asymmetrical rolling devices.

Article first published online: xxxx
Manuscript Revised: April 6, 2017
Manuscript Received: January 30, 2017

[1] A. Sato, E. Chishima, K. Soma, T. Mori, *Acta Metall*. **1982**, *30*, 1117.
[2] J. Van Humbeeck, *Adv. Eng. Mater.* **2001**, *3*, 11.
[3] Q. Gu, J. Van Humbeeck, L. Delaey, *J. Phys. IV France* **1994**, *C3*, 135.
[4] A. Sato, E. Chishima, Y. Yamaji, T. Mori, *Acta Metall*. **1984**, *32*, 539.
[5] O. Matsumura, S. Furusako, T. Furukawa, H. Oysuka, *ISIJ Int*. **1996**, *36*, 1103.
[6] O. Matsumura, S. Furusako, T. Sumi, T. Furukawa, H. Otsuka, *Mater. Sci. Eng. A* **1999**, *272*, 459.
[7] N. Stanford, D. Dunne, *Mater. Sci. Eng. A* **2006**, *422*, 352.
[8] H. Fu, H. Zhao, S. Song, Z. Zhang, J. Xie, *J. Alloys Compd*. **2016**, *686*, 1008.
[9] A. Druker, C. Sobrero, H.-G. Brokmeier, J. Malarría, R. Bolmaro, *Mater. Sci. Eng. A* **2008**, *481–482*, 578.
[10] C. Lee, B. Duggan, *Metall. Trans*. **1991**, *22A–11*, 2637.
[11] A. Bintu, G. Vincze, R. Picu, A. Lopes, *Mater. Des*. **2016**, *100*, 151.
[12] S. Li, N. Qin, J. Liu, X. Zhang, *Mater. Des*. **2016**, *90*, 1010.
[13] W. Li, Y. Shen, C. Xie, *Mater. Des*. **2016**, *105*, 404.
[14] M. Lobanov, S. Danilov, V. Pastukhov, S. Averin, Y. Khrunyk, A. Popov, *Mater. Des*. **2016**, *109*, 251.
[15] Q. Zhao, Z. Liu, S. Li, T. Huang, P. Xia, L. Lu, *J. Alloys Compd*. **2017**, *691*, 786.
[16] X. Zhang, Q. Yan, S. Lang, Y. Wang, C. Ge, *Mater. Des*. **2016**, *109*, 443.
[17] S. Sahoo, R. Sabat, S. Sahni, S. Suwas, *Mater. Des*. **2016**, *91*, 58.
[18] B. Yu, P. Pei, B. Yu, D. Li, X. Zhang, J. Huang, H. Ding, S. Chen, Y. Zhu, *Adv. Eng. Mater.* **2016**, *18*, 5.

DOI: 10.1002/adem.201700062

[19] J. Sidor, R. Petrov, L. Kestens, *Adv. Eng. Mater.* **2011**, *13*, 10.
[20] L. Tóth, *Adv. Eng. Mater.* **2003**, *5*, 5.
[21] R. Jahadi, M. Sedighi, H. Jahed, *Mater. Sci. Eng. A* **2014**, *593*, 178.
[22] S. Agnew, P. Mehrotra, T. Lillo, G. Stoica, P. Liaw, *Acta Mater.* **2005**, *53*, 11.
[23] A. Rebhi, T. Makhlouf, N. Njah, Y. Champion, J. Couzinié, *Mater. Charact*. **2009**, *60*, 1489.
[24] S. Suwas, R. Massion, L. Tóth, J. Fundenberger, B. Beausir, *Mater. Sci. Eng. A* **2009**, *520*, 134.
[25] O. Higuera-Cobos, J. Berríos-Ortiz, J. Cabrera, *Mater. Sci. Eng. A* **2014**, *609*, 273.
[26] N. De Vincentis, A. Kliauga, M. Ferrante, M. Avalos, H.-G. Brokmeier, R. Bolmaro, *Mater. Charact*. **2015**, *107*, 98.
[27] W. Zhang, L. Jiang, N. Li, Y. Wen, *J. Mater. Process. Technol*. **2008**, *208*, 130.
[28] H. Bernardi, K. Käfer, L. Naito, J. Otubo, *Mater. Sci. Forum* **2013**, *738–739*, 252.
[29] A. V. Druker, A. Baruj, L. Isola, V. Fuster, J. Malarría, R. Bolmaro, *Mater. Des*. **2016**, *107*, 153.
[30] E. M. Mielnik, *Metalworking Science and Engineering*, McGraw-Hill Inc., New York **1991**.
[31] N. Bergeon, *PhD Thesis*, Lyon **1996**.
[32] J. Kallend, U. Kocks, A. Rollett, H. Wenk, *Mater. Sci. Eng. A* **1991**, *132*, 1.
[33] S. Lundberg, *Scand. J. Metall*. **2004**, *33*, 129.
[34] C. W. MacGregor, L. F. Coffin, *J. Appl. Mech*. **1943**, *10*, A13.

DOI: 10.1002/adem.201700062